JACS
JOURNAL OF THE AMERICAN CHEMICAL SOCIETY
Article
pubs.acs.org/JACS

Elucidating the Link between NMR Chemical Shifts and Electronic Structure in d^0 Olefin Metathesis Catalysts

Stéphanie Halbert,[†,#] Christophe Copéret,[*,§] Christophe Raynaud,[*,†] and Odile Eisenstein[*,†,‡]

[†]Institut Charles Gerhardt, UMR 5253 CNRS, cc 1501, Université de Montpellier, Place. E. Bataillon, F-34095 Montpellier, France
[§]ETH Zürich, Department of Chemistry and Applied Sciences, Vladimir Prelog Weg 1-5, 10, CH-8093 Zürich, Switzerland
[‡]Centre for Theoretical and Computational Chemistry (CTCC), Department of Chemistry, University of Oslo, P.O. Box 1033, Blindern, 0315 Oslo, Norway

Supporting Information

ABSTRACT: The nucleophilic carbon of d^0 Schrock alkylidene metathesis catalysts, [M] = CHR, display surprisingly low downfield chemical shift (δ_{iso}) and large chemical shift anisotropy. State-of-the-art four-component relativistic calculations of the chemical shift tensors combined with a two-component analysis in terms of localized orbitals allow a molecular-level understanding of their orientations, the magnitude of their principal components ($\delta_{11} > \delta_{22} > \delta_{33}$) and associated δ_{iso}. This analysis reveals the dominating influence of the paramagnetic contribution yielding a highly deshielded alkylidene carbon. The largest paramagnetic contribution, which originates from the coupling of alkylidene σ_{MC} and π^*_{MC} orbitals under the action of the magnetic field, is analogous to that resulting from coupling σ_{CC} and π^*_{CC} in ethylene; thus, δ_{11} is in the MCH plane and is perpendicular to the MC internuclear direction. The higher value of carbon-13 δ_{iso} in alkylidene complexes relative to ethylene is thus due to the smaller energy gap between σ_{MC} and π^*_{MC} vs this between σ_{CC} and π^*_{CC} in ethylene. This effect also explains why the highest value of δ_{iso} is observed for Mo and the lowest for Ta, the values for W and Re being in between. In the presence of agostic interaction, the chemical shift tensor principal components orientation (δ_{22} or δ_{33} parallel or perpendicular to π_{MX}) is influenced by the MCH angle because it determines the orientation of the alkylidene CHR fragment relative to the MC internuclear axis. The orbital analysis shows how the paramagnetic terms, understood with a localized bond model, determine the chemical shift tensor and thereby δ_{iso}.

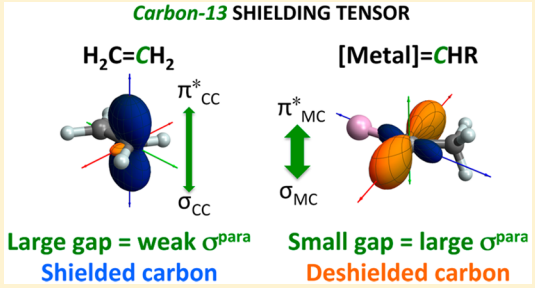

INTRODUCTION

Metal alkylidene complexes have been an intense area of research in the past 50 years, because they are key reactants and/or intermediates in alkene metathesis,[1] cyclopropanation[2] and pseudo-Wittig[3] reactions as well as in alkane homologation reactions such as alkane metathesis[4] and hydrogenolysis;[4c,d,5] they have also been proposed to intervene in the Fischer–Tropsch process and related reactions.[6] Detailed structural analyses of well-defined d^0 group 6 and 7 transition metal alkylidene complexes have appeared over the years because of their key importance as highly active molecular and supported alkene metathesis catalysts.[5,7−9] They display several structural peculiarities, in terms of bonding situation and spectroscopic signatures. Besides the expected short MC bond distance, representative of a multiple bond, these systems exist as mixture of *syn* and *anti* isomers, with a preference for the former. These structural preferences are typically associated with the presence of an α-M···CH agostic interaction, which can be evidenced by specific signatures, such as wide MCC and associated acute MCH bond angles according to X-ray and neutron diffraction,[10a,b] low ν_{C-H} stretching frequencies and perturbed NMR signatures (lower J_{CH} and upfield carbon chemical shift).[10c,d] In particular, the J_{CH} coupling constant can adopt low to very low values (80−120 Hz)[3,11] as a result of the α-M···CH agostic interaction. Of special interest for the present work, all alkylidene carbons are associated with highly deshielded carbon, typically found between 200 and 300 ppm, and a very large "span" (400−500 ppm). The highly deshielded carbon, similar to what is observed for carbocation,[12] may be very surprising since d^0 metal alkylidenes are highly nucleophilic groups and usually described with a carbanionic resonance structure explaining their reactivity toward carbonyl compounds in the pseudo-Wittig reactions or their protonation by weak acids such as alcohols or surface and molecular silanols.[13]

In this work, we provide molecular insight onto the origin of the highly deshielded chemical shift by analyzing the values and the orientations of the principal components of the chemical shift tensor of the alkylidene ligand on a series of alkylidene catalysts. The calculations are based on models of a set of isostructural silica-supported d^0 metal alkylidene complexes, (≡SiO)(X)M(E)(=CH*t*Bu) (Figure 1), for which the principal components of the tensor have been recently measured.[7] All experimental complexes share the same

Received: December 2, 2015
Published: January 19, 2016

DOI: 10.1021/jacs.5b12597
J. Am. Chem. Soc. 2016, 138, 2261−2272

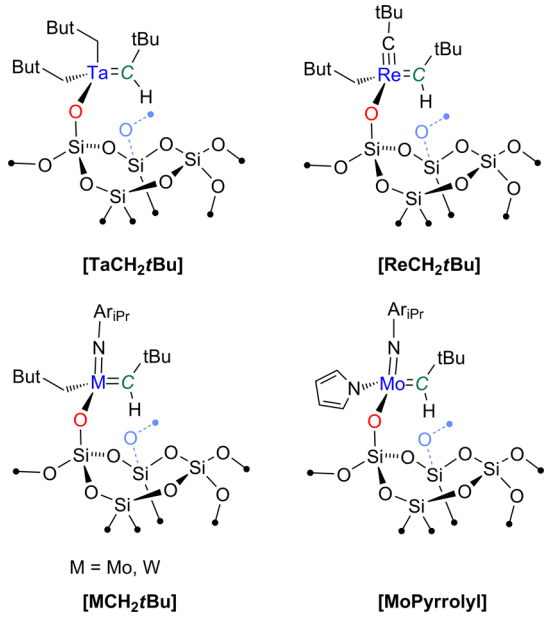

Figure 1. Well-defined silica-supported alkylidene metal complexes; the *syn* confirmation was experimentally determined for Mo, W and Re but not for Ta (to be addressed in this work).

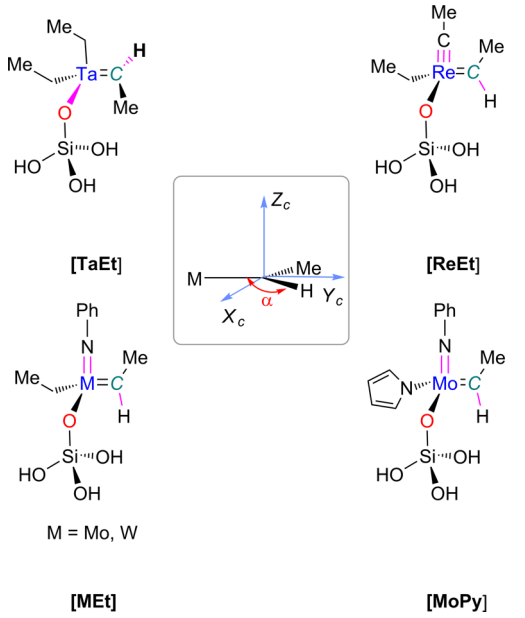

Figure 2. Computational models of the experimental complexes showing the more stable *syn* configuration according to calculations. The axes used for describing the shielding tensors are shown in the inlet.

alkylidene function and differ by the nature of the metal and the ancillary ligands, with M(E) = $TaCH_2tBu$, MoNAr, WNAr or ReC*t*Bu and X = alkyl or pyrrolyl (Figure 1). Solid state NMR measurements on the ^{13}C alkylidene carbon in these supported complexes have given information on the components of the chemical shifts, and thus on δ_{iso} and δ_{aniso}, albeit partially averaged by residual dynamics, in particular for Ta and Re.[7] To better grasp the electronic features of these alkylidene groups that could be derived from the analysis of the NMR data, we use ethylene as a reference because ethylene and the alkylidene complexes bear sp^2 carbon group, albeit in very different electronic environments.[14] Ethylene was chosen as a reference because its NMR properties have been studied in depth, in particular through the measurement and calculations of its chemical shift tensor.[14] Furthermore, the nature of the alkyl group on the alkylidene carbon should only marginally perturb the local electron environment. Thus, this study aims at obtaining a molecular-level understanding of how the metal fragment bonded to an sp^2 carbon modifies its electronic environment, by calculating and analyzing the chemical shift tensor at this carbon.

Calculations of NMR chemical shifts of light atoms in the presence of heavy atoms are presently possible for systems of reasonably large size.[15] Here, we combine state-of-the-art calculations of the chemical shift tensor with 4-component (4c) Hamiltonian and an analysis of 2-component (2c) NMR shielding tensor in terms of scalar relativistic localized orbitals of the contribution of the various bonds to the NMR chemical shift at this atom. This computational analysis, has been carried out for molecules with main group atoms[16] and only for few systems containing transition metal atoms.[17] In the present case, this analysis should inform on the influence of the metal and ligands as well as structural features on the magnitude and orientations of the chemical shift tensor for these alkylidene carbons, effects which are still not understood.

COMPUTATIONAL DETAILS

Models. The supported catalysts of Figure 1 were modeled by the molecular systems, [**MR**] shown in Figure 2, because they describe well the electronic features of a surface siloxy ligand as previously validated[7,9,18] and allow the highest level of calculations of the NMR chemical shifts in computationally accessible time to be carried out. For this purpose, all *t*Bu groups were replaced by Me groups. Test calculations with *t*Bu in place of Me on the alkyl derivative of the molybdenum complex [**MoR**] was shown to increase the carbon chemical shift by 8 ppm in good agreement with the increase of isotropic chemical shift of around 10 ppm observed under such substitution, (Table S13 in the Supporting Information).

Computational Level. The structures of [**MR**] were optimized with the B3PW91 functional,[19] the quasi-relativistic SDD effective core potential (ECP)[20] for Mo, W, Re and Ta, completed by the associated basis-set and a 6-31(d,p) basis set for C, N, O, Si and H[21] using the Gaussian09 program.[22] Geometry optimization of the most stable structure of all complexes with a triple-ζ basis set (def2-TZVPP) was shown to give essentially identical geometries (see Supporting Information, Table S11). For the determination of the potential energy surface associated with the MCH angle, all structural parameters were optimized for each value of the MCH angle, which was varied by 5° step between 130 and 70°.

The NMR shielding constants of the alkylidene carbon were computed using the gauge-including atomic orbital (GIAO) method[23] with a 4-component (4c) fully relativistic Hamiltonian and the B3PW91 hybrid functional with the Dirac 2013 program.[24] While previous studies have been often carried out with GGA functionals, we chose a hybrid functional because it better describes the electronic structure of metal containing species. A Dyall triple-ζ basis set was used for the metallic centers,[25] whereas lighter atoms were described by uncontracted pc-S2 basis sets.[26] The simple magnetic balance (sMB) scheme recently proposed by Olejniczak et al.[27] was used.

Quasi-relativistic single point calculations were also performed using ADF[28] program, with the one-parameter hybrid B1PW91[29] functional and Slater-type orbital basis sets of triple-ζ polarized (TZ2P)[30] quality. Relativistic effects were treated by the 2-component (2c) zeroth-order regular approximation (ZORA),[31] and GIAO were used for calculating the NMR shieldings. It should be noted that using the geometries obtained with the def2-TZVPP basis set resulted in isotropic chemical

DOI: 10.1021/jacs.5b12597
J. Am. Chem. Soc. 2016, 138, 2261−2272

Table 1. Calculated and Experimental ^{13}C Ethylidene NMR Chemical Shift Tensors for the *syn* and *anti* Configuration of Complexes of Figure 2[a]

[MR]	ΔE[b] kcal/mol	α_{opt}[c] deg	carbon charge[d]	method	δ_{11} ppm	δ_{22} ppm	δ_{33} ppm	δ_{iso} ppm	δ_{aniso} ppm
$[MoPy]_s$	0.0	104.0	−0.320	2c[e]	680	113	92	295	385
				4c[f]	682	121	97	300	382
$[MoPy]_a$	2.9	123.2	−0.317	2c	722	146	66	311	411
				4c	724	154	74	317	407
$[MoPy]_e$				exp	603	181	71	285	318
$[MoEt]_s$	0.0	103.9	−0.356	2c	652	105	95	284	368
				4c	655	114	101	290	365
$[MoEt]_a$	2.4	123.7	−0.347	2c	690	133	67	297	393
				4c	693	141	77	304	389
$[MoEt]_e$				exp	574	156	107	279	295
$[WEt]_s$	0.0	104.7	−0.505	2c	566	122	66	251	315
				4c	571	143	75	263	308
$[WEt]_a$	2.6	123.5	−0.491	2c	599	105	86	264	336
				4c	604	126	103	278	326
$[WEt]_e$				exp	429	219	117	255	174
$[ReEt]_s$	0.0	106.7	−0.381	2c	565	108	62	245	320
				4c	563	113	56	244	319
$[ReEt]_a$	1.8	127.7	−0.367	2c	579	133	33	248	331
				4c	577	139	26	247	330
$[ReEt]_{e/s}$				exp	372	239	130	247	125
$[ReEt]_{e/a}$					NA	NA	NA	257	NA
$[TaEt]_s$	0.0	87.8	−0.657	2c	479	219	−18	227	252
				4c	493	240	−9	241	252
$[TaEt]_a$	3.7	120.4	−0.707	2c	568	146	49	255	314
				4c	584	171	68	274	310
$[TaEt]_e$				exp	394	205	136	245	149
C_2H_4	–	121.8	−0.428	2c	259	121	14	131	128
				4c	264	128	16	136	128
$[C_2H_4]_e$[14]				exp	234	120	24	126	108[g]
					239	129	29	132[g]	106[g]

[a]Ethylene is provided as reference. [b]Energies relative to the more stable isomer. See text for description of the geometries (*syn*: s, *anti*: a, exp: e). [c]MCH angle, CCH for ethylene. [d]NBO charge at alkylidene carbon with 2c calculations. [e]2c calculations. [f]4c calculations. [g]Values calculated from the reported principal components of the chemical shifts.

shifts differing by less than 5 ppm for the five complexes studied in this work (Table S12 in the Supporting Information).

Chemicals shifts as defined in eq 1 were computed for the carbon alkylidene relative to tetramethylsilane (TMS) at the same level of theory. The isotropic carbon shielding, defined also in eq 1 is 183.7 and 190.1 ppm for TMS at the 4c and 2c level of calculations, respectively.

$$\begin{pmatrix} \delta_{11} & 0 & 0 \\ 0 & \delta_{22} & 0 \\ 0 & 0 & \delta_{33} \end{pmatrix} = \sigma_{iso}^{ref} \cdot \begin{pmatrix} 1 & 0 & 0 \\ 0 & 1 & 0 \\ 0 & 0 & 1 \end{pmatrix} - \begin{pmatrix} \sigma_{11} & 0 & 0 \\ 0 & \sigma_{22} & 0 \\ 0 & 0 & \sigma_{33} \end{pmatrix}$$

$$\delta_{iso} = 1/3(\delta_{11} + \delta_{22} + \delta_{33}) \quad (1)$$

Analyses of atomic charges and of natural localized molecular orbitals were done with the NBO 6.0 program.[32,33] The NMR shielding tensors calculated with the quasi-relativistic 2-component Hamiltonian were analyzed using scalar-relativistic natural localized molecular orbitals.[34] For convenience, we refer to this LMO analysis of chemical shift as the natural chemical shift analysis (NCS) using the terminology proposed in the original work by Weinhold et al.,[34a] which was at the origin of further developments.[34b−d] The analysis of the orbital current densities for the 2c shielding tensor was validated by showing that the spin−orbit (SO) contributions are small relative to the paramagnetic terms. Thus, the 1c shielding tensors, obtained by representing the relativistic effects only through quasi-relativistic ECP, are similar to the 2c results and subsequent NCS analysis shows similar trends for the diamagnetic and paramagnetic contributions (Table S10 and Figure S15 in Supporting Information). In this work, the sum of the two contributions (paramagnetic and SO) are reported. The graphical representations of NMR carbon shielding tensors was obtained with the procedure and tools described earlier.[35]

Additional technical aspects, useful for the reading of this work, are defined here. Orthonormal reference axes (X_c, Y_c, and Z_c) centered on the carbon are used for describing the shielding tensor (Figure 2). The X_c axis lies in the alkylidene plane and is perpendicular to the M−C axis, Y_c is along the M−C direction and Z_c is perpendicular to the alkylidene plane and thus parallel to the metal−alkylidene π-bond. The principal components of the shielding tensor, ranked in increasing shielding order, are $\sigma_{11} < \sigma_{22} < \sigma_{33}$. They form an orthonormal set with directions that are close to the X_c, Y_c, and Z_c in many systems (see Figures S12 and S13 in the Supporting Information)

RESULTS

Structural Features. In all complexes of Figure 2, the d^0 metal center has pseudotetrahedral coordination, but the alkylidene group adopts a preferred orientation relative to the other ligands.[9,13b] For the imido Mo or W and the alkylidyne Re complexes, the alkylidene ligand is coplanar with the imido or alkylidyne ligand. In addition, the alkylidene methyl substituent is *syn*, i.e., it points toward these multiply bonded ligands as observed experimentally, $[MR]_s$.[9,18] In the Ta complex, the alkylidene ligand is coplanar with the Ta−O bond and the alkylidene methyl substituent is *syn* to the Ta−O bond.

DOI: 10.1021/jacs.5b12597
J. Am. Chem. Soc. 2016, 138, 2261−2272

In addition, another conformation in which the ethylidene is rotated by 180° (*anti* isomer) is found to be a secondary minimum, [**MR**]$_a$, 1.8 to 3.7 kcal/mol above the *syn* isomer (Table 1).

In both *syn* and *anti* configurations, a conjugation is established between the π orbitals of the alkylidene and imido (respectively alkylidyne) via a metal d orbital of adapted symmetry. In the case of the Ta complex, a p lone pair of the siloxy group is involved in the conjugation. In the *syn* configuration, the C−H bond is antiperiplanar to either the M−N (imido), M−C (alkylidyne), or M−O (siloxy) σ-bonds, respectively (shown in magenta in Figure 2). This arrangement maximizes the hyperconjugation between the alkylidene σ-C−H bond and the low-lying M−N, M−C or M−O empty orbitals—also called antibonds—as revealed by the NBO analysis (Table S1). Thus, for the *syn* conformation, the alkylidene C−H bond is delocalized for almost 11% in the Ta−O antibond, while these values are significantly lower for Mo−N, W−N and Re−C (4% and 3% respectively). This delocalization is not present in the *anti* conformation. Electron poor metal centers favor the delocalization of electron density and thus the decrease of the MCH α angle, which is the manifestation of an agostic interaction.[36] Such small α angle is only found in the *syn* configuration in the present systems. The optimized MCH angles, α_{opt} in Table 1, are similar for [**MoR**]$_s$, [**WEt**]$_s$, and [**ReEt**]$_s$ (104.0°, 104.7°, and 106.7°, respectively) and significantly smaller for [**TaEt**]$_s$ (87.8°).

The NBO analysis reveals that the positive charge at the metal is indeed the largest for Ta (1.84) and the smallest for Re (1.04) with intermediate values for W (1.59) and Mo (1.39 and 1.28 for [**MoPy**]$_s$ and [**MoEt**]$_s$, respectively). This charge evolution, all considerably smaller than the corresponding formal oxidation numbers, are determined by the electron-donating ability of the two ancillary ligands that differ in these complexes. Both, imido and alkylidyne ligands donate electron density to the metal center via a σ-bond and two d_π−p_π interactions but the latter ligand is a better donor than the former. Likewise, the pyrrolyl ligand is less good electron donor than an alkyl group. The Ta atom receives the least density from its two alkyl ligands, because the single bonded alkyl ligand is a less good donor than a multiply bonded ligand like imido or alkylidyne. These effects apply to a large range of MCH angles as revealed by the shallowness of the potential energy surfaces around the minimum for all these complexes in the *syn* configuration (Figure S1 in Supporting Information). While it is well-accepted that agostic interactions occurring only in the *syn* configuration should lower the corresponding alkylidene J_{CH} coupling constant,[9] the effect of agostic interaction on the carbon chemical shift and its anisotropy is not yet understood.

Chemical Shifts for Equilibrium Structures. The chemical shift anisotropy (CSA) reflects the orientation dependence of the chemical shift (δ)—or the corresponding shielding (σ)—with respect to the external magnetic field B_0 due to the anisotropic electron distribution. The chemical shift is described by a second rank tensor, with principal components ($\delta_{11} > \delta_{22} > \delta_{33}$, i.e., with increasing shieldings $\sigma_{11} < \sigma_{22} < \sigma_{33}$). In solution, the chemical shift interaction is averaged by molecular tumbling to the isotropic chemical shift δ_{iso}, eq 1. In solids, the CSA gives rise to characteristic powdered patterns, reflecting its tensor nature. Using the Haeberlen convention,[34] the width of the spectra is related to the chemical shift anisotropy δ_{aniso} (eq 2), which measures how sensitive the interaction is to the orientation of the magnetic field.

$$\delta_{aniso} = \delta_{ii} - \delta_{iso} \quad (2)$$

and ($|\delta_{ii} - \delta_{iso}| > |\delta_{22} - \delta_{iso}| > |\delta_{jj} - \delta_{iso}|$) with $i = 1$ or 3 and $j \neq i$.

Ethylene being a highly relevant reference system, the chemical shift tensor of the ethylene carbon, determined experimentally,[14] was calculated at the present level of calculation. The 4c calculations give an isotropic chemical shift of 136 ppm and δ_{11}, δ_{22} and δ_{33} values of 264, 128, and 16 ppm, respectively, compare well to the experimental isotropic chemical shifts of 132 ppm (in argon matrix at 15 K) and principal components of 239, 129, 29 ppm (Table 1). Experiment showed that the intermediate component, δ_{22} is along the CC axis and that the most shielded component is perpendicular to the molecular plane (parallel to the π-bond), resulting in the most deshielded component to be contained in the molecular plane and to be perpendicular to the CC direction. Calculations agree with these attributions. The 3-D representation of the shielding tensor for carbon, (Figure 3), indicates the direction of shielding (along Z_c) with blue and orange colors for shielding and deshielding relative to a bare carbon nucleus, respectively.

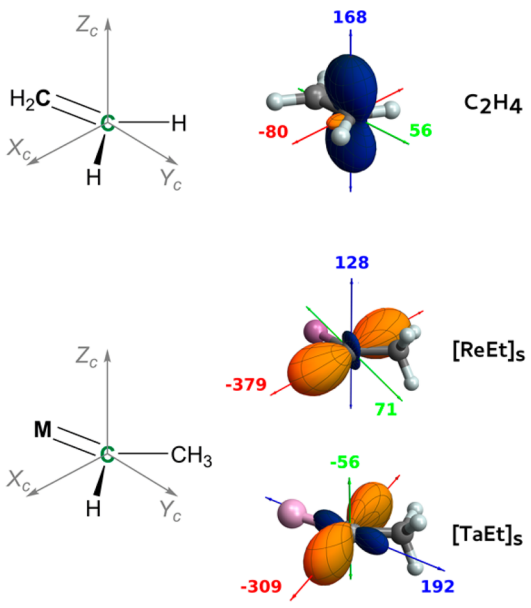

Figure 3. Calculated shielding tensors represented as polar plots of functions $\sum_{ij} r_i r_j \sigma_{ij}$.[35]

The principal components of the chemical shift tensors for the ethylidene carbon in the *syn* and *anti* configurations of Figure 2 with the 4c calculations are given in Table 1. The isotropic chemical shifts, δ_{iso}, are in the 200−300 ppm range, in good agreement with the experimental values. The chemical shifts are ca. 10 ppm downfield (i.e., too large) with the exception of the tantalum complex. These calculations were carried out for ethylidene complexes while the experimental values correspond to neopentylidene complexes which would increase the chemical shifts by a further 8 ppm. Thus, the differences between calculated and experimental values are within 20 ppm of a 200−400 ppm scale. Nonetheless, the trends are well reproduced. For instance, the isotropic chemical shift of the molybdenum complex is higher than that of the

DOI: 10.1021/jacs.5b12597
J. Am. Chem. Soc. 2016, 138, 2261−2272

tungsten by 24 ppm (exp) vs 27 ppm (calc.). Note also that the values for δ_{aniso}, calculated at the static limit, are larger than the experimental values because of the residual dynamics, as previously discussed.[7] The calculations reproduce well *the accepted yet surprising* downfield shift by more than 100 ppm of the alkylidene carbon relative to that of ethylene. The deshielding of the alkylidene carbon relative to that of ethylene has indeed no relation with the electron density at the carbon as can be seen by the NBO charges at the alkylidene which can be close to that ethylene (≈ −0.4 for Mo and Re) or considerably more negative (≈ −0.7 for Ta).

Shielding Tensors. A 3D graphical representation of the shielding tensors at the alkylidene carbon for Re and Ta (Figure 3 and Figure S14 for other complexes, see also Table 1 for chemical shifts) illustrates the important decreased shielding at the carbon that results from the presence of the metal fragment. The large blue volume, indicating shielding, along Z_c, is strongly decreased and in contrast, a large orange volume (indicating deshielding) with its main component in the alkylidene plane essentially along X_c is present for all systems. Some shielding survives though and the direction of maximum shielding depends on the metal; it is in the Z_c direction for Re (i.e., along the Re=C π-bond) and approximately in the Y_c direction (i.e., along the M−C σ-bond) for Ta. The directions for the principal components for all systems are shown in the Supporting Information (Table S2 and Figures S6−S8). While the most deshielded component remains essentially along X_c for all systems including ethylene, the orientation of the other two components can be along either of the two Y_c and Z_c axes or even tilted relative to them. A consequence is that for some species, the orientations of the two more shielded principal components is as in ethylene (i.e., δ_{22} is along Y_c and δ_{33} along Z_c). This is the case notably of the Re complex at equilibrium geometry. In other complexes the orientations of these two more shielded principal components differ from that of ethylene like in the Ta complex where δ_{22} and δ_{33} are along the Z_c and Y_c axes, respectively at equilibrium geometry. While, it is tempting to categorize the alkylidene complexes using the orientations of the two more shielded components, this may be challenging because of the significant tilt of the principal components δ_{22} and δ_{33} relative to Y_c and Z_c in several cases.

Thus, the most significant difference between the NMR responses of an ethylene carbon and a metal alkylidene carbon is the occurrence of very large deshielding essentially in the X_c direction and a decrease (in a smaller extend) of the shielding in the other directions. The large increase of deshielding in the X_c direction is, in the major part, responsible for observing the chemical shifts of the alkylidene carbons in the 200−300 ppm range. The chemical shifts reported in Table 1 show that the decreases of shielding along X_c of 230 to 420 ppm, contributes by 70−140 ppm to δ_{iso}, (eq 1) that are 100 to 170 ppm higher than in ethylene.

Influence of MCH Bond Angles at the Alkylidene on the Chemical Shifts. We evaluated the influence of α, used as a descriptor of agostic interaction, on the carbon alkylidene chemical shift in the *syn* configuration of complexes of Figure 2. The 4c calculations show only a moderated influence of α on the isotropic chemical shifts (Figure 4a and Figure S4, Table S3). For all systems, δ_{iso} diminishes slightly in a monotonous manner upon decreasing α over the 130° to 70° range: the diminution is almost negligible in the case of $[\mathbf{ReEt}]_s$ and somewhat larger for the Mo complexes with the largest decrease (50 ppm, Figure S4) being for $[\mathbf{MoPy}]_s$. In sharp

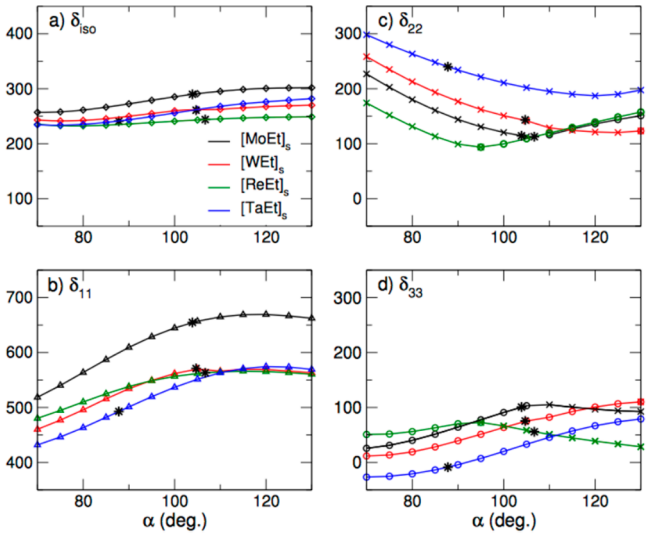

Figure 4. (a) Isotropic chemical shifts and values of the principal components ($\delta_{11} > \delta_{22} > \delta_{33}$) of the chemical shift tensors as a function of the MCH α angle (deg). Triangles indicate a principal component directed along X_c, circles along Y_c and crosses along Z_c. While δ_{11} is essentially along X_c for all systems, δ_{22} and δ_{33} are not aligned with either Y_c or Y_c in some cases. In these cases, the labeling corresponds to the closest attribution. The orientation of all components is given in the Supporting Information (Table S2). See Figure 2 for labels of chemical species.

contrast, the α angle has a much greater influence on the individual principal components δ_{11}, δ_{22} and δ_{33} (Figure 4b−d and Figure S5). The most deshielded component δ_{11} decreases strongly as α decreases. The two other components vary in lesser magnitude and in somewhat opposite manner; they also vary in a nonmonotonous manner for some metals such as Re and Mo (it is also associated with a change in the orientation of δ_{22} and δ_{33} in some cases, vide infra). The sum of these two components is dominated by δ_{22} and thus opposes the influence of δ_{11} that still dominates resulting in an increased shielding at the alkylidene carbon with decreasing α. This is somewhat paradoxical since an agostic interaction to a d^0 metal is associated with slight loss of electron density at the carbon as confirmed by NBO (Table S9), which could have been expected to lead to deshielding. In order to determine if the C−H bond had a specific role to play, we evaluated the effect of decreasing the ReCMe angle in the *anti* isomer $[\mathbf{ReEt}]_a$ (Figure S11), even if it is not energetically favored. It resulted in similar trends for the chemical shift tensors as obtained with the decrease of the ReCH angle in the *syn* isomer. Therefore, the changes in the chemical shift tensor upon decrease of the MCH angle is not determined by the agostic CH interaction per se.

NCS Analysis of the Chemical Shift Tensor Principal Components. The nature—values and orientation—of the chemical shift tensor of the alkylidene carbon is related to the electronic structure at the carbon atom. Natural chemical shift (NCS) analysis, based on the natural bond orbital (NBO) analysis method,[16,34] allows establishing a link between NMR chemical shifts and chemical (electronic) structures. Because this analysis is not yet possible for electronic structures calculated with the 4c Hamiltonian, all chemical shifts were recalculated with 2c Hamiltonian (see Computational Details); they yield chemical shifts only slightly changed relative to the 4c-calculations (Table 1) but make them amenable for an NCS analysis. The NCS analysis was carried out for the alkylidene

DOI: 10.1021/jacs.5b12597
J. Am. Chem. Soc. 2016, 138, 2261−2272

Table 2. NCS Analysis of the σ^{p+SO} Contributions of the Principal Components of the Shielding Tensor with the 2c Calculations[a]

		σ_{11}				σ_{22}				σ_{33}			
[MR]	α (deg)	σ_{MC}	π_{MC}	σ_{CC}	σ_{CH}	σ_{MC}	π_{MC}	σ_{CC}	σ_{CH}	σ_{MC}	π_{MC}	σ_{CC}	σ_{CH}
$[\mathbf{MoPy}]_s$	104.0	−456	−148	−95	−31	−53	7	−45	−53	−19	16	−55	−83
$[\mathbf{MoPy}]_a$	123.2	−475	−161	−59	−80	0	9	−99	−110	−46	0	−14	−31
$[\mathbf{MoEt}]_s$	103.9	−443	−142	−91	−31	−72	1	−32	−25	0	19	−64	−103
$[\mathbf{MoEt}]_a$	123.7	−465	−150	−57	−76	0	8	−92	−102	−47	0	−12	−31
$[\mathbf{WEt}]_s$	104.7	−399	−108	−81	−21	−92	−5	−18	−15	0	22	−54	−96
$[\mathbf{WEt}]_a$	123.5	−419	−117	−46	−67	−17	7	−67	−77	−57	−2	−17	−31
$[\mathbf{ReEt}]_s$	106.7	−389	−129	−75	−26	−2	14	−69	−115	−65	0	−15	−19
$[\mathbf{ReEt}]_a$	127.7	−397	−130	−42	−68	−2	9	−100	−102	−40	1	−1	−29
$[\mathbf{TaEt}]_s$	87.8	−334	−78	−108	0	−131	−7	−49	−21	2	33	−20	−59
$[\mathbf{TaEt}]_a$	120.4	−402	−97	−51	−62	−115	−4	7	−22	−4	18	−57	−65
		σ_{11}				σ_{22}				σ_{33}			
	α (deg)	σ_{CC}	π_{CC}	σ_{CH}	σ_{CH}	σ_{CC}	π_{CC}	σ_{CH}	σ_{CH}	σ_{CC}	π_{CC}	σ_{CH}	σ_{CH}
C_2H_4	121.8	−189	−12	−47	−47	0	14	−98	−98	−29	0	−4	−4

[a]The values of diamagnetic, paramagnetic and total values of the principal components are given in Table S5.

carbon for all *syn*- and *anti*-complexes. This analysis was also carried to understand the effect of a change of the MCH angle in the *syn* isomer (associated with the presence of an agostic interaction) through a study of the entire range of α values between 130° and 70°. A small grid of 10° was used for Re while calculations for the other metal centers were limited to α = 70, 100 and 130° and α_{opt}. The results are given in Table 2 and Tables S5−S7. Following previous studies, the NCS analysis will be discussed in terms of shielding σ_C.[34]

The NCS analysis divides the shielding into diamagnetic, paramagnetic and spin−orbit (SO) contributions, (eq 3):

$$\sigma_C = \sigma_C{}^{d} + \sigma_C{}^{p+SO} \quad (3)$$

The diamagnetic term contributes to the *shielding* of the nucleus and arises from the ability of the external magnetic field to generate a circulation of charges in the ground-state electron distribution. In contrast, the paramagnetic part contributes to the *deshielding* of the nucleus and arises from the ability of the external magnetic field to force the electrons to circulate through the molecules by making use of virtual orbitals.[16,34] The calculated $\sigma_C{}^{d}$ are remarkably similar for all three components of the chemical shift tensor (Table S5), and more importantly also similar for all complexes and ethylene with differences no larger than 20 ppm. For instance, the diamagnetic contribution to the shielding along the X_c axis varies between 238 and 245 ppm for the entire series of alkylidene complexes. For a given complex such as $[\mathbf{TaEt}]_s$ the diamagnetic contributions are 241, 216, and 273 ppm along the three axes, while the corresponding paramagnetic terms are −530, −247 and −66 ppm. Therefore, the paramagnetic term determines the anisotropy of the shielding tensor whose principal components are −289, −31 and 208 ppm. The situation is also similar for ethylene where the diamagnetic terms are 246, 248, and 216 ppm, and the paramagnetic terms are −316, −179 and −39 ppm; thus yielding highly anisotropic shielding tensor with principal components of −69, 69, and 177 ppm. Thus, the differences in ^{13}C chemical shifts of the various metal alkylidene complexes, the large increase in chemical shift (deshielding) of the alkylidene complexes relative to ethylene and the global asymmetry of the chemical shift tensor around this sp^2 carbon resides mainly in the paramagnetic term $\sigma_C{}^{p+SO}$.

The paramagnetic contributions are the result of a current density J_p induced by the applied external magnetic field B_0. This induced current density J_p stems from the orbitals, which in the absence of the external field, are occupied or empty.

The induced current density moves in the plane perpendicular to B_0 containing the alkylidene carbon center, and the resulting induced field is parallel and adds to B_0, hence inducing so-called an increase in chemical shift, also called deshielding or downfield shift. Within the GIAO framework, the action of the magnetic field (for instance along X_c if this axis is along one of the principal components of the tensor) is proportional to that of L_x, the angular momentum operator along the X_c-axis, on each atomic orbital about its respective center. Following Cornwell's model of orbital rotations, the action of L_i (i = 1, 2 or 3, where these axes are along the principal components of the shielding) couples an occupied orbital ψ_{occ} and with a vacant orbital ψ_{vac}; it can be visualized as a 90° rotation about one of the axes of an occupied orbital ψ_{occ}, lying in a plane perpendicular to this axis. If the rotated orbital $L_i|\psi_{occ}$ overlaps with a vacant orbital ψ_{vac}, this results in a local induced field approximately proportional to the value given in eq 4.[15,16,34]

$$\frac{\langle\psi_{vac}|L_i|\psi_{occ}\rangle\langle\psi_{vac}|L_i/r^3|\psi_{occ}\rangle}{\Delta E_{vac-occ}} \quad (4)$$

This term is denoted $\{\psi_{vac}|\psi_{occ}\}$ thereafter. Therefore, the induced shift depends on the overlap between the rotated occupied and the empty orbitals, and is inversely proportional to the difference in energy between the two orbitals involved, $\Delta E_{vac\text{-}occ}$. The largest total paramagnetic contribution is associated with the most deshielded principal component since the diamagnetic term is essential equal for the three components. The NCS analysis (Table 2) show that all bonds located at the alkylidene carbon, i.e., σ_{MC}, π_{MC}, σ_{CC} and σ_{CH}, and associated antibonds σ^*_{MC}, π^*_{MC}, σ^*_{CC} and σ^*_{CH} participate to the paramagnetic term. For ethylene, the corresponding orbitals are σ_{CC}, π_{CC}, as well as the two σ_{CH} bonds and their associated antibonds. We can use ethylene to present the essential features of the analysis that will be developed below in full for the alkylidene complexes. The energy criterion of eq 4 indicates that the largest influence is associated with the frontier or near-frontier orbitals. This gives

DOI: 10.1021/jacs.5b12597
J. Am. Chem. Soc. 2016, 138, 2261−2272

an essential role to σ_{CC} and π_{CC} and associated antibonds σ^*_{CC} and π^*_{MC}. These orbitals are coupled via the angular momentum L_x, parallel to X_c (Scheme 1). Table 2 shows the

Scheme 1. Schematic Localized Orbitals Contributing to the Shielding of the Carbon in Ethylene along X_c

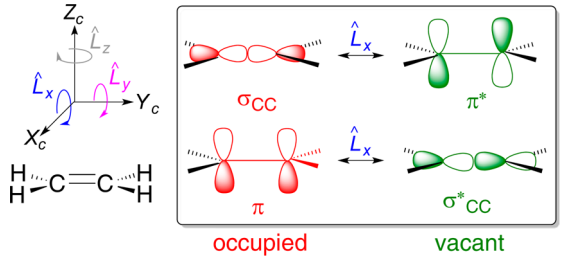

dominating influence of σ_{CC} over π_{CC} (−189 vs −12 ppm). This leads to maximum deshielding in the direction of X_c, i.e., in the molecular plane of ethylene and perpendicular to the CC axis. This results in the orange lobe on the ethylene carbon as shown in Figure 3. Other directions of the tensor are more shielded and in particular the direction of the π bond. The lowest paramagnetic contribution is along Z_c. This originates from the fact that L_z couples occupied (σ_{CC} and σ_{CH}) to empty orbitals (σ^*_{CC} and σ^*_{CH}) in the plane of ethylene that are well separated in energy and have a small overlap because of the 120° CCH and HCH bond angles. This accounts in full for the ordering of the three principal components of the shielding tensor for ethylene, as illustrated in Figure 3 and established experimentally.[14]

Results are similar for the alkylidene complexes. The frontier and near-frontier orbitals σ_{MC} and π_{MC} and corresponding antibonds σ^*_{MC} and π^*_{MC} are associated with the most deshielded component of the shielding tensor. These orbitals are coupled via the angular moment operator L_1, which is, essentially along the X_c axis in all cases, and is thus assigned as L_x (Scheme 2). Calculations show that the direction of the most deshielded principal component does not deviate from the X_c axis by more than a few degrees in all cases (see Figure S6 for a graphical representation of the orientation of the most deshielded principal component as a function of α).[37] The resulting induced current produces a magnetic field that adds to the magnetic field applied along the X_c axis, hence an important deshielding in this direction that does not exist in the two other directions of the principal components.

The two more shielded components σ_{22} and σ_{33} are in the plane perpendicular to the direction of σ_{11} and thus essentially in the plane defined by the Y_c and Z_c axes, i.e., containing the MC internuclear direction and M=C π-bond (Scheme 2). However, their orientations within the Y_cZ_c plane vary with the metal center and the MCH α angle. For instance, in the case of [**ReEt**]$_s$, σ_{22} and σ_{33} are essentially along Y_c and Z_c respectively when $\alpha \geq \alpha_{opt}$ (106.7°). In contrast, for the tantalum complex, σ_{22} and σ_{33} are along Z_c and Y_c, respectively at any α angle. For the tungsten complex at equilibrium geometry, σ_{22} and σ_{33} are strongly tilted away from the W−C σ- and π-bonds. The influence of the MCH angle on the orientations of σ_{22} and σ_{33} is also noticeable; for MCH angle smaller than 90°, σ_{22} and σ_{33} are along the Z_c and Y_c axes, respectively for all complexes. However, for MCH angle larger than 90°, the situation is more diverse. Thus, in [**ReEt**]$_s$, there is a significant reorientation of the two more shielded components as the MCH angle

Scheme 2

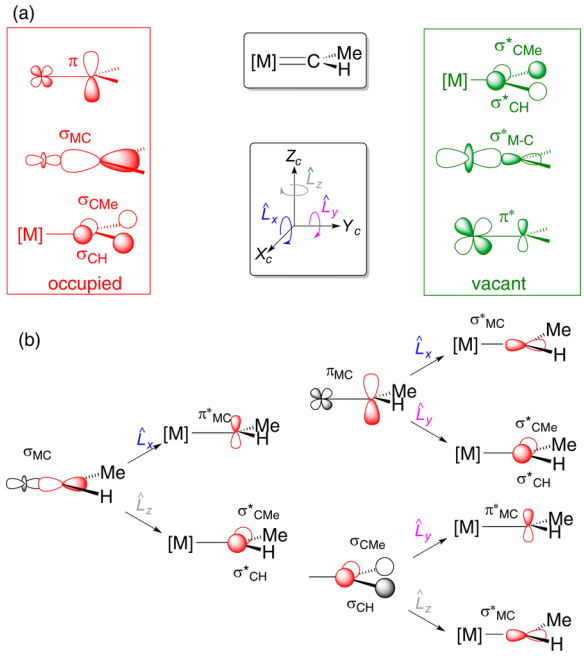

Localized orbitals involved in the paramagnetic contribution of the shielding at the alkylidene carbon. (a) Occupied, empty orbitals and system of axes. (b) Schematic representation of the action of the angular momentum operator (L_i with $i = x, y$ and z) coupling occupied and empty orbitals for selected orbitals that contribute to the paramagnetic term to the shielding at the alkylidene carbon.

decreases. However, for the tantalum complexes there is no reorientation of these two components. For the Mo and W complexes, there is also some reorientation but the situation is even more complex since the deviations away from Y_c and Z_c of these components at large MCH angle are significant. Complete description of the orientation of the tensor components is given in the Supporting Information (Figures S7 and S8).

The NCS analysis carried out for all metal alkylidene complexes in various geometries give the contribution of occupied orbitals, σ_{MC}, π_{MC}, σ_{CH}, σ_{CC} in each case.[38] Consequently, it is possible to analyze the contributions of each orbital using the rotations of orbitals about the X_c, Y_c and Z_c axes as schematically represented in Scheme 2, but only when the principal components are aligned with these axes. When the components deviate from these directions, combinations of rotations are needed and a qualitative description is possible, but harder to establish.

We will thus focus on the cases where the three components are mostly aligned with the axes. This occurs in sufficient number of cases to allow us to construct a qualitative understanding of the orientation and magnitude of the principal components of the shielding tensor. It should be remembered that it is sufficient to consider the paramagnetic term since the diamagnetic term is essentially the same for all systems considered in this study. The use of NCS allows in particular to understand (i) the deshielding of the alkylidene carbon relative to the ethylene carbon (ii) the influence of the metal on the magnitude of deshielding and (iii) the influence of the MCH angle, and thus of the agostic interaction on the magnitude of the shielding and orientation of the principal components.

DOI: 10.1021/jacs.5b12597
J. Am. Chem. Soc. 2016, 138, 2261−2272

(i) The alkylidene carbon of the metal alkylidene complexes is strongly deshielded relative to that of an olefin (ethylene here). We have mentioned earlier that the most deshielded component σ_{11} is driving the isotropic shift. It determines the deshielding of the carbon of the metal alkylidene. As mentioned above, the paramagnetic term of σ_{11} is associated with the coupling of the frontier and near-frontier orbitals, i.e., the coupling of σ_{MC} with π^*_{MC}, $\{\pi^*_{MC}|\sigma_{MC}\}$, and π_{MC} with σ^*_{MC}, $\{\sigma^*_{MC}|\pi_{MC}\}$. The NCS analysis (Table 2) indicates that the absolute value of the first of these two terms is larger than the second one (300−475 ppm and less than 200 ppm, respectively); consequently, we will focus on the first term $\{\pi^*_{MC}|\sigma_{MC}\}$. Table 2 shows also that its absolute value is considerably larger (from 300 to 500 ppm) than the corresponding term in ethylene $\{\pi^*_{CC}|\sigma_{CC}\}$, (<200 ppm). This difference originates from the smaller energy gap between occupied and empty orbitals in M═C vs C═C double bonds. The effect of the overlap is harder to evaluate since the σ_{MC} is more localized on carbon than on metal but the reverse applies π^*_{MC}.

(ii) A similar argument can be used for rationalizing the relative chemical shifts associated with different metals. The calculations and the experimental results show that the chemical shift of the carbon in the Mo complexes is the most downfield of all alkylidene complexes (290−300 ppm). This is associated with an absolute value of the paramagnetic contribution for σ_{11}, which is higher than 700 ppm, while it is below this value for all other complexes (Table S5). This is itself determined by the absolute value of $\{\pi^*_{MC}|\sigma_{MC}\}$, which is larger than 400 ppm for Mo complexes and smaller for all other complexes. Since the energy of 4d orbitals are lower than that of 5d orbitals, the energy gap between σ_{MC} orbital localized on the carbon and the empty π^*_{MC} orbital localized on a metal is smaller for a 4d than 5d metal complex.[39] This accounts for the more important deshielding carbon in Mo alkylidene complexes. Among the three metal alkylidene 5d metal centers, the alkylidene carbon of the tantalum complex appears to have a larger shielding than the two other complexes. This is associated with the smallest absolute value of σ_{11} at a given α angle relative to the W and Re complexes. Tantalum being more electropositive than W and Re, π^*_{MC} is at higher energy and this increases the energy gap associated with the coupling term $\{\pi^*_{MC}|\sigma_{MC}\}$, hence a decrease of the absolute value of the paramagnetic contribution.

(iii) Concerning the change in chemical shielding with MCH α angle, as mentioned above, the lowering in the chemical shift δ_{iso} when α decreases is also determined by the lowering of δ_{11} (Figure 4 and Figure S5): the carbon becomes increasingly shielded as the MCH angle decreases. For the same rhenium complex, Table S6 shows that, in this case also, the term that determines the increase in shielding for σ_{11} is the diminution of the absolute value of the paramagnetic term $\{\pi^*_{MC}|\sigma_{MC}\}$. This is the case for all metal alkylidene complexes (Table S7) and is illustrated graphically in Figure 5 for the rhenium complex.

Scheme 2 provides an orbital interpretation of the result presented in (iii). Since L_x acts perpendicularly to the Y_cZ_c plane, the maximum coupling between σ_{MC} with π^*_{MC} occurs when σ_{MC} lies in the Y_cZ_c plane. This is the case when the sp^n carbon hybrid that forms σ_{MC} points toward M i.e., when the MCH angle is around 120° (Scheme 3b left-hand side). This is no longer the case when the MCH angle is significantly less than 120°. The direction of this sp^n hybrid orbital is determined by the MeCH angle. Since it remains constant as α varies, the sp^n hybrid at the alkylidene carbon tilts away from pointing toward M. Thus, for small values of α the hybrid orbital that forms the M−C σ-bond is no longer contained in the Y_cZ_c plane and it contributes to σ_{11} only via its projection on this plane (in pink on Scheme 3b right-hand side). This necessarily decreases the absolute value of $\{\pi^*_{MC}|\sigma_{MC}\}$ and this is significant for $\alpha < 90°$.

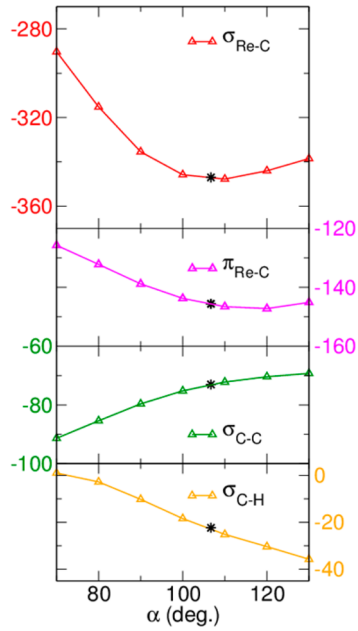

Figure 5. Contribution of the bonds at the alkylidene carbon to σ_{11} in $[\mathbf{ReEt}]_s$ as a function of the MCH α angle.

Scheme 3. Qualitative Representations of Occupied (Red) And Empty (Blue) Orbitals Coupled to Contribute to (a) σ_{zz} and (b) σ_{xx}

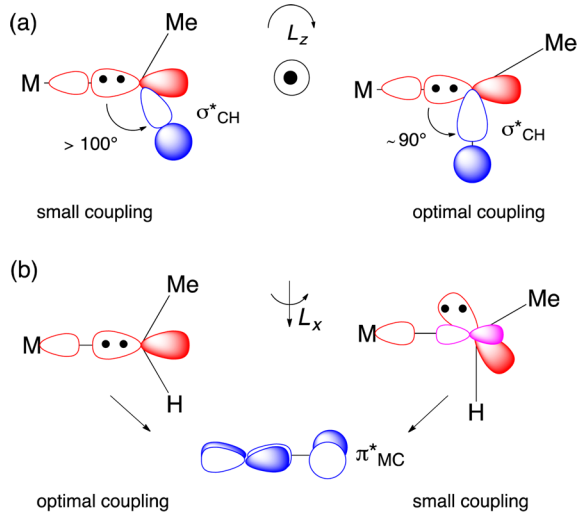

DOI: 10.1021/jacs.5b12597
J. Am. Chem. Soc. 2016, 138, 2261−2272

The contributions of other orbitals to σ_{11} also vary but to a lesser extent (Figure 5). It is interesting to note that the absolute value of the σ_{CMe} bond contribution increases as α decreases because the MCMe angle increases, hence the projection of σ_{CMe} on the MC interatomic direction increases. In parallel, the absolute value of σ_{CH} contribution decreases at small α angle because the C−H bond has a very small projection on the MC axis. These two last variations are overall small and it is clear that $\{\pi^*_{MC}|\sigma_{MC}\}$ dominates the decrease of the absolute value of σ_{11} shifts the metal alkylidene to more shielded position. This rationalizes the low chemical shift of 203 ppm, in a tantalum complex with a very strong α CH agostic interaction.[11]

Worthy of note the variation of the chemical shift at the carbon is thus essentially determined by the M−C bond and is hardly influenced by the C−H bond hence by the agostic interaction. This accounts for the similarities in the results obtained with the *syn* and *anti* isomers of the rhenium complex.

The two more shielded components σ_{22} and σ_{33} can only easily be analyzed when they are along Y_c and Z_c. We will thus limit the discussion to the rhenium and tantalum complexes for which it is the case (Tables S6 and S7, Figures S7, S8 and S10 in Supporting Information). We will focus on discussing why $[\mathbf{ReEt}]_s$ has the most shielded component along Z_c when α is equal or larger than α_{opt} and along Y_c when $\alpha < 90°$. We will also discuss why in the case of the tantalum complex the most shielded component is along Y_c for all values of α.

For the rhenium complex, at equilibrium structure (α = 106.7°), the NCS analysis shows that the orbitals that mainly contribute to the parametric term of σ_{22} (parallel to Y_c) are σ_{CH} (−115 ppm) and σ_{CC} (−69 ppm) while those which contribute to σ_{33} (parallel to Z_c) are distributed among the three σ bonds at the alkylidene carbon, σ_{MC} (−65 ppm), σ_{CH} (−19 ppm) and σ_{CC} (−15 ppm) (Table S6). The deshielding along Y_c comes from the coupling of σ_{CH} and σ_{CC} via L_y with π^*_{ReC}, while the deshielding along Z_c comes from the coupling of σ and σ^* bonds in the alkylidene plane via L_z. Since the energy gap between occupied and empty orbitals is larger for the latter the deshielding along Y_c is more important than along Z_c. The shielding along Y_c and Z_c are thus σ_{22} and σ_{33}, respectively. The results are similar for α larger than the equilibrium value. However, for a small α angle (<90°), the main contributions to σ_{22} (parallel to Z_c) are σ_{ReC} (−121 ppm for α = 70°) and σ_{CC} (−66 ppm) while that to σ_{33} (parallel to Y_c) is mainly σ_{CH} (−93 ppm) with some contribution of σ_{CC} (−30 ppm). The reason why there is now more deshielding along Z_c is that the bond angle close to 90° between MC and CH increases the coupling between σ_{ReC} and σ^*_{CH} via the L_z angular momentum (Scheme 3a). The same applies for the coupling between σ_{CC} and σ^*_{CH}. In contrast the deshielding along Y_c is the smallest, since only σ_{CH} can couple efficiently with π^*_{MC} via the L_y angular momentum because the C−H bond is essentially perpendicular to the MC direction. Similar arguments apply to the tantalum complex but in this case all empty orbitals involving Ta are higher in energy (Table S7). This increases the energy gap involving any empty orbital with a metal contribution. The consequence is that for large α angles, the deshielding along Y_c is smaller since it involves the coupling of σ_{CH} and σ_{CC} with π^*_{TaC} while the deshielding along Z_c is less affected since no empty orbital involving the metal is involved. It results that the deshielding along Y_c is less that along Z_c and consequently σ_{22} is along Z_c and σ_{33} along Y_c at large α angle. For small α angles, the σ_{22} and σ_{33} components are along Z_c and Y_c, respectively as obtained with the rhenium complex since the higher energy of π^*_{TaC} can only decrease the already smallest deshielded contribution.

The effect of the metal on the shielding tensor can thus be summarized as follows. Raising the energy level of the metal d orbitals decreases the paramagnetic contribution to the shielding in all directions for any MCH angle. This decrease of deshielding is affecting least the Z_c direction. Consequently, since the deshielding remains still important for σ_{11}, the shielding along Z_c appears as the σ_{22} component of the shift tensor for any MCH angle. The reverse applies when the metal orbitals are lower in energy; they can more efficiently contribute to the paramagnetic term. This not only leads to increased global deshielding at the alkylidene carbon but more specifically to an order of increasing shielding along the directions $X_c < Y_c$ and $< Z_c$ for large MCH angle ($\geq\alpha_{opt}$). Thus, the directions of the σ_{22} and σ_{33} components may change with MCH angle for the complexes with relatively low d orbitals since in all cases, the σ_{33} component is along the Y_c direction, for small MCH angles.

CONCLUSIONS

In this study, we have sought the link between the NMR signatures and the electronic structures of d^0 olefin catalysts of 4d- and 5d-metals (Ta, Mo, W and Re). The NMR chemical shift of the alkylidene carbon appears strongly downfield-shifted, i.e., in the region where carbocations are typically observed, although the alkylidene ligand in these d^0 Schrock type metal complexes are known to bear a nucleophilic character. In addition, the solid state NMR spectra of these alkylidene carbons display large chemical shift anisotropy with a particularly deshielded δ_{11} component, illustrating a strong anisotropy in the electron distribution around carbon.

State-of-the-art quantitative 4 component (4c) relativistic calculations of the shielding tensor on a large series of d^0 alkylidene complexes, including *syn* and *anti* isomers as well as intermediate structures with various MCH bond angles, reproduce well the experimental values for the three components of the chemical shift tensor (δ_{11}, δ_{22} and δ_{33}). The NCS analysis using 2 component (2c) relativistic calculations provide molecular-level understanding of the directions and the magnitude of the shielding tensor principal components and associated isotropic chemical shift (average value). These studies reveal the following salient features:

(i) All complexes have their most deshielded component in the plane of the alkylidene =CHR fragment perpendicular to the MC interatomic direction ($\delta_{11} = \delta_{xx}$). This is analogous to what is found for ethylene for which the most deshielded component is in the molecular plane perpendicular to the CC interatomic direction. The orientation of two other components, δ_{22} and δ_{33}, depends however on the metal complexes.

(ii) The downfield shift of the alkylidene carbon by 100 to 200 ppm with respect to ethylene is in large part due to the most deshielded component δ_{11}, which is shifted by 200 to 400 ppm downfield relative to that of ethylene.

(iii) The chemical shift tensor is found to be sensitive to the MCH bond angle. For a small MCH bond angle (<90°) the most deshielded component δ_{11} is still in the plane of the alkylidene and perpendicular to the M=C π-bond but is moved significantly upfield. Furthermore, the most shielded component δ_{33} is along the MC internuclear

DOI: 10.1021/jacs.5b12597
J. Am. Chem. Soc. 2016, 138, 2261−2272

direction and the intermediate δ_{22} component along the alkylidene π-bond.

Analysis of the chemical shifts reveal first that there is no direct relation between the charge at carbon and the chemical shift in these alkylidene complexes. Further analysis of the shielding tensor using the NCS method associated with the NBO analysis, carried out on 2 component (2c) relativistic calculations (validated by comparison with the 4c calculations), shows that the diamagnetic contribution, associated with shielding, is similar in all alkylidene complexes *and* ethylene. Thus, it cannot explain the observed chemical shift differences among the series and between them and ethylene, pointing out that the difference must mainly arise from the paramagnetic term, which is associated with deshielding.

The largest paramagnetic term in the alkylidene complexes arises from a coupling of σ_{MC} and π^*_{MC} orbitals and determines σ_{11}: it is considerably larger for all alkylidene metal complexes (typically between 500 and 700 ppm) than for ethylene (around 300 ppm), for which σ_{11} arises from the coupling of σ_{CC} and π^*_{CC} orbitals. This large difference originates from the smaller energy gap between occupied and empty orbitals in the metal alkylidene complexes. Additional more subtle differences between the NMR shielding in metal complexes can also be rationalized using the same arguments, by looking at the coupled—occupied and empty—localized orbitals and the energy gap between them. For instance, the very deshielded isotropic chemical shift observed for Mo by comparison with its isoelectronic W and Re complexes, which mainly results from the highly deshielded σ_{xx} component, is the consequence of the lower-lying empty orbitals for 4d (Mo) vs 5d metals (W and Re). This also explains why Ta complexes, the most electropositive metal of the series, show the most upfield alkylidene chemical shift; its higher energy empty orbitals containing a metal contribution lead to inefficient coupling and consequently lower deshielding and lower chemical shift values. Related reasoning rationalizes all other variations in chemical shifts, in particular with respect to the variation of MCH angle, and accounts for the upfield shift of δ_{11} and the possible change of direction of δ_{22} and δ_{33} at small MCH angle, typically associated in the alkylidene complexes with α-agostic C−H bond. Worthy of note the change of tensor orientation is not determined by the M···H interaction per se, but only by the orientation of the alkylidene−CH(R) fragment with respect to the internuclear M−C direction (in the alkylidene X_cY_c plane). The coupling between carbon based σ-orbitals and σ^* orbitals is enhanced when two bonds make a 90° angle resulting in the paramagnetic term to be larger in absolute value in the direction of the metal−alkylidene π-bond than along the internuclear MC direction. This leads to the most shielded component σ_{33} to lie along the M−C σ-bond. Thus, all systems with an acute MCH have the intermediate component σ_{22} along the metal−alkylidene π-bond.

This analysis shows how the paramagnetic term, which can be fully understood with a localized orbital model, determines the main properties of the chemical shift tensor. A similar reasoning is possible for a wide number of organometallic systems and offers the possibility for a chemical understanding of the origin of the NMR chemical shifts and electronic structure of carbon directly bonded to metals. We are currently exploring this field, and will report our advances in due course.

■ ASSOCIATED CONTENT

Supporting Information

The Supporting Information is available free of charge on the ACS Publications website at DOI: 10.1021/jacs.5b12597.

Additional figures, tables, Cartesian coordinates of optimized structures and energies (in a.u.). (PDF)

■ AUTHOR INFORMATION

Corresponding Authors

*ccoperet@ethz.ch

*christophe.raynaud1@umontpellier.fr

*odile.eisenstein@univ-montp2.fr

Present Address

#Université Pierre et Marie Curie−Paris 06 (UPMC), UMR 7616, Laboratoire de Chimie Théorique, Sorbonne Universités, F-75005, Paris, France.

Notes

The authors declare no competing financial interest.

■ ACKNOWLEDGMENTS

S. H. thanks the Ministère de l'Enseignement Supérieur et de la Recherche (MESR) for a Ph.D. fellowship. The authors thank IDRIS and CINES for a generous computational time through DARI project number x2016087529.

■ REFERENCES

(1) (a) Schrock, R. R.; Hoveyda, A. H. *Angew. Chem., Int. Ed.* **2003**, *42*, 4592. (b) Schrock, R. R. *Angew. Chem., Int. Ed.* **2006**, *45*, 3748. (c) Grubbs, R. H. *Angew. Chem., Int. Ed.* **2006**, *45*, 3760. (d) Schrock, R. R. *Chem. Rev.* **2009**, *109*, 3211. (e) Meek, S. J.; O'Brien, R. V.; Llaveria, J.; Schrock, R. R.; Hoveyda, A. H. *Nature* **2011**, *471*, 461. (f) Hoveyda, A. H. *J. Org. Chem.* **2014**, *79*, 4763. (g) *Handbook of Metathesis*, 2nd ed.; Grubbs, R. H., Wenzel, A. G., O'Leary, D. J., Khosravi, E., Eds.; Wiley-VCH: Weinheim, 2015.

(2) (a) Davies, H. M. L.; Alford, J. S. *Chem. Soc. Rev.* **2014**, *43*, 5151. (b) Doyle, M. P. *J. Org. Chem.* **2006**, *71*, 9253. (c) Lebel, H.; Marcoux, J. F.; Molinaro, C.; Charette, A. B. *Chem. Rev.* **2003**, *103*, 977. (d) Timmons, D. J.; Doyle, M. P. *J. Organomet. Chem.* **2001**, *617*, 98.

(3) Nugent, W. A.; Mayer, J. M. *Metal-Ligand Multiple Bonds*; Wiley: New York, 1988.

(4) (a) Copéret, C.; Maury, O.; Thivolle-Cazat, J.; Basset, J.-M. *Angew. Chem., Int. Ed.* **2001**, *40*, 2331. (b) Le Roux, E.; Chabanas, M.; Baudouin, A.; de Mallmann, A.; Copéret, C.; Quadrelli, E. A.; Thivolle-Cazat, J.; Basset, J.-M.; Lukens, W.; Lesage, A.; Emsley, L.; Sunley, G. J. *J. Am. Chem. Soc.* **2004**, *126*, 13391. (c) Basset, J.-M.; Copéret, C.; Soulivong, D.; Taoufik, M.; Thivolle-Cazat, J. *Acc. Chem. Res.* **2010**, *43*, 323. (d) Copéret, C. *Chem. Rev.* **2010**, *110*, 656. (e) Chen, Y.; Abou-Hamad, E.; Hamieh, A.; Hamzaoui, B.; Emsley, L.; Basset, J.-M. *J. Am. Chem. Soc.* **2015**, *137*, 588.

(5) Chabanas, M.; Vidal, V.; Copéret, C.; Thivolle-Cazat, J.; Basset, J.-M. *Angew. Chem., Int. Ed.* **2000**, *39*, 1962.

(6) (a) Leconte, M. *J. Mol. Catal.* **1994**, *86*, 205−220. (b) Maitlis, P. M. *J. Organomet. Chem.* **2004**, *689*, 4366.

(7) Blanc, F.; Basset, J.-M.; Copéret, C.; Sinha, A.; Tonzetich, Z. J.; Schrock, R. R.; Solans-Montfort, X.; Clot, E.; Eisenstein, O.; Lesage, A.; Emsley, L. *J. Am. Chem. Soc.* **2008**, *130*, 5886.

(8) (a) Chabanas, M.; Quadrelli, E. A.; Fenet, B.; Copéret, C.; Thivolle-Cazat, J.; Basset, J.-M.; Lesage, A.; Emsley, L. *Angew. Chem., Int. Ed.* **2001**, *40*, 4493. (b) Chabanas, M.; Baudouin, A.; Copéret, C.; Basset, J.-M. *J. Am. Chem. Soc.* **2001**, *123*, 2062. (c) Chabanas, M.; Baudouin, A.; Copéret, C.; Basset, J.-M.; Lukens, W.; Lesage, A.; Hediger, S.; Emsley, L. *J. Am. Chem. Soc.* **2003**, *125*, 492. (d) Blanc, F.; Copéret, C.; Thivolle-Cazat, J.; Basset, J.-M.; Lesage, A.; Emsley, L.; Sinha, A.; Schrock, R. R. *Angew. Chem., Int. Ed.* **2006**, *45*, 1216. (e) Rhers, B.; Salameh, A.; Baudouin, A.; Quadrelli, E. A.; Taoufik, M.;

DOI: 10.1021/jacs.5b12597
J. Am. Chem. Soc. 2016, 138, 2261−2272

Copéret, C.; Lefebvre, F.; Basset, J.-M.; Solans-Monfort, X.; Eisenstein, O.; Lukens, W.; Lopez, L. P. H.; Sinha, A.; Schrock, R. R. *Organometallics* **2006**, *25*, 3554. (f) Blanc, F.; Thivolle-Cazat, J.; Basset, J.-M.; Copéret, C.; Hock, A. S.; Tonzetich, Z. J.; Schrock, R. R. *J. Am. Chem. Soc.* **2007**, *129*, 1044.
(9) (a) Solans-Monfort, X.; Clot, E.; Copéret, C.; Eisenstein, O. *Organometallics* **2005**, *24*, 1586. (b) Poater, A.; Solans-Monfort, X.; Clot, E.; Copéret, C.; Eisenstein, O. *Dalton Trans.* **2006**, 3077.
(10) (a) Schultz, A. J.; Williams, J. M.; Schrock, R. R.; Rupprecht, G. A.; Fellmann, J. D. *J. Am. Chem. Soc.* **1979**, *101*, 1593. (b) Schultz, A. J.; Brown, R. K.; Williams, J. M.; Schrock, R. R. *J. Am. Chem. Soc.* **1981**, *103*, 169. (c) Schrock, R. R.; Crowe, W. E.; Bazan, G. C.; DiMare, M.; O'Regan, M. B.; Schofield, M. H. *Organometallics* **1991**, *10*, 1832. (d) Oskam, J. H.; Schrock, R. R. *J. Am. Chem. Soc.* **1993**, *115*, 11831.
(11) Freundlich, J. S.; Schrock, R. R.; Davis, W. M. *Organometallics* **1996**, *15*, 2777.
(12) Haw, J. F.; Song, W. G.; Marcus, D. M.; Nicholas, J. B. *Acc. Chem. Res.* **2003**, *36*, 317.
(13) (a) Rendón, N.; Blanc, F.; Copéret, C. *Coord. Chem. Rev.* **2009**, *253*, 2015. (b) Schrock, R. R. *Chem. Rev.* **2009**, *109*, 3211.
(14) (a) Zilm, K. W.; Conlin, R. T.; Grant, D. M.; Michl, J. *J. Am. Chem. Soc.* **1980**, *102*, 6672. (b) Zilm, K. W.; Grant, D. M. *J. Am. Chem. Soc.* **1981**, *103*, 2913.
(15) For selected papers, see: (a) Helgaker, T.; Jaszuński, M.; Ruud, K. *Chem. Rev.* **1999**, *99*, 293. (b) Autschbach, J. *Struct. Bonding (Berlin, Ger.)* **2004**, *112*, 1. (c) Feindel, K. W.; Wasylishen, R. E. *Can. J. Chem.* **2004**, *82*, 27. (d) Kaupp, M.; Bühl, M.; Malkin, V. G. *Calculations of NMR and EPR Parameters: Theory and Applications*; Wiley-VCH: Weinheim, 2006. (e) Casabianca, L. B.; de Dios, A. C. *J. Chem. Phys.* **2008**, *128*, 052201. (f) Widdifield, C. M.; Shurko, R. W. *Concepts Magn. Reson., Part A* **2009**, *34*, 91. (g) Autschbach, J.; Zheng, S. *Annu. Rep. NMR Spectrosc.* **2009**, *67*, 1. (h) Hrobárik, P.; Hrobárikova, V.; Meier, F.; Repisky, M.; Kaupp, M. *J. Phys. Chem. A* **2011**, *115*, 5654. (i) Wodyński, A.; Gryff-Keller, A.; Pecul, M. *J. Chem. Theory Comput.* **2013**, *9*, 1909. (j) Greif, A. H.; Hrobárik, P.; Hrobáriková, V.; Arbuznikov, A. V.; Autschbach, J.; Kaupp, M. *Inorg. Chem.* **2015**, *54*, 7199.
(16) (a) Bohmann, J. A.; Farrar, T. C. *J. Phys. Chem.* **1996**, *100*, 2646. (b) Wiberg, K. B.; Hammer, J. D.; Zilm, K. W.; Cheeseman, J. R. *J. Org. Chem.* **1999**, *64*, 6394. (c) Auer, D.; Strohmann, C.; Arbuznikov, A. V.; Kaupp, M. *Organometallics* **2003**, *22*, 2442. (d) Auer, D.; Kaupp, M.; Strohmann, C. *Organometallics* **2004**, *23*, 3647. (e) Auer, D.; Kaupp, M.; Strohmann, C. *Organometallics* **2005**, *24*, 6331. (f) Standara, S.; Bouzková, K.; Straka, M.; Zacharová, Z.; Hocek, M.; Marek, J.; Marek, R. *Phys. Chem. Chem. Phys.* **2011**, *13*, 15854. (g) Toušek, J.; Straka, M.; Sklenář, V.; Marek, R. *J. Phys. Chem. A* **2013**, *117*, 661. (h) Vummaleti, S. V. C.; Nelson, D. J.; Poater, A.; Gómez-Suárez, A.; Cordes, D. B.; Slawin, A. M. Z.; Nolan, S. P.; Cavallo, L. *Chem. Sci.* **2015**, *6*, 1895.
(17) (a) Ruiz-Morales, Y.; Schreckenbach, G.; Ziegler, T. *Organometallics* **1996**, *15*, 3920. (b) Wu, G.; Rovnyak, D.; Johnson, M. J.; Zanetti, N. C.; Musaev, D. G.; Morokuma, K.; Schrock, R. R.; Griffin, R. G.; Cummins, C. C. *J. Am. Chem. Soc.* **1996**, *118*, 10654. (c) Ruiz-Morales, Y.; Schreckenbach, G.; Ziegler, T. *J. Phys. Chem.* **1996**, *100*, 3359. (d) Sceats, E. L.; Figueroa, J. S.; Cummins, C. C.; Loening, N. M.; Van der Wel, P.; Griffin, R. G. *Polyhedron* **2004**, *23*, 2751. (e) Autschbach, J.; Zheng, S. *Magn. Reson. Chem.* **2008**, *46*, S45. (f) Rossini, A. J.; Mills, R. W.; Briscoe, G. A.; Norton, E. L.; Geier, S. J.; Hung, I.; Zheng, S.; Autschbach, J.; Schurko, R. W. *J. Am. Chem. Soc.* **2009**, *131*, 3317. (g) Zhu, J.; Kurahashi, T.; Fujii, H.; Wu, G. *Chem. Sci.* **2012**, *3*, 391. (h) Pascual-Borràs, M.; López, X.; Rodríguez-Fortea, A.; Errington, R. J.; Poblet, J. M. *Chem. Sci.* **2014**, *5*, 2031. (i) Pascual-Borràs, M.; López, X.; Poblet, J. M. *Phys. Chem. Chem. Phys.* **2015**, *17*, 8723. (j) Vícha, J.; Straka, M.; Munzarová, M. L.; Marek, R. *J. Chem. Theory Comput.* **2014**, *10*, 1489.
(18) (a) Solans-Monfort, X.; Eisenstein, O. *Polyhedron* **2006**, *25*, 339. (b) Solans-Monfort, X.; Filhol, J.-S.; Copéret, C.; Eisenstein, O. *New J. Chem.* **2006**, *30*, 842.
(19) (a) Becke, A. D. *J. Chem. Phys.* **1993**, *98*, 5648−5652. (b) Perdew, J. P.; Wang, Y. *Phys. Rev. B: Condens. Matter Mater. Phys.* **1992**, *45*, 13244.
(20) Andrae, D.; Häußermann, U.; Dolg, M.; Stoll, H.; Preuß, H. *Theor. Chim. Acta* **1990**, *77*, 123.
(21) Hariharan, P. C.; Pople, J. A. *Theor. Chim. Acta* **1973**, *28*, 213.
(22) Frisch, M. J.; Trucks, G. W.; Schlegel, H. B.; Scuseria, G. E.; Robb, M. A.; Cheeseman, J. R.; Scalmani, G.; Barone, V.; Mennucci, B.; Petersson, G. A.; Nakatsuji, H.; Caricato, M.; Li, X.; Hratchian, H. P.; Izmaylov, A. F.; Bloino, J.; Zheng, G.; Sonnenberg, J. L.; Hada, M.; Ehara, M.; Toyota, K.; Fukuda, R.; Hasegawa, J.; Ishida, M.; Nakajima, T.; Honda, Y.; Kitao, O.; Nakai, H.; Vreven, T.; Montgomery, J. A., Jr.; Peralta, J. E.; Ogliaro, F.; Bearpark, M.; Heyd, J. J.; Brothers, E.; Kudin, K. N.; Staroverov, V. N.; Kobayashi, R.; Normand, J.; Raghavachari, K.; Rendell, A.; Burant, J. C.; Iyengar, S. S.; Tomasi, J.; Cossi, M.; Rega, N.; Millam, J. M.; Klene, M.; Knox, J. E.; Cross, J. B.; Bakken, V.; Adamo, C.; Jaramillo, J.; Gomperts, R.; Stratmann, R. E.; Yazyev, O.; Austin, A. J.; Cammi, R.; Pomelli, C.; Ochterski, J. W.; Martin, R. L.; Morokuma, K.; Zakrzewski, V. G.; Voth, G. A.; Salvador, P.; Dannenberg, J. J.; Dapprich, S.; Daniels, A. D.; Farkas, Ö.; Foresman, J. B.; Ortiz, J. V.; Cioslowski, J.; Fox, D. J. *Gaussian 09*, Revision D01; Gaussian, Inc.: Wallingford, CT, 2009.
(23) (a) Ditchfield, R. *J. Chem. Phys.* **1972**, *56*, 5688. (b) Lee, A. M.; Handy, N. C.; Colwell, S. M. *J. Chem. Phys.* **1995**, *103*, 10095.
(24) Visscher, L.; Jensen, H. J. Aa; Bast, R.; Saue, T.; Bakken, V.; Dyall, K. G.; Dubillard, S.; Ekström, U.; Eliav, E.; Enevoldsen, T.; Faßhauer, E.; Fleig, T.; Fossgaard, O.; Gomes, A. S. P.; Helgaker, T.; Lærdahl, J. K.; Lee, Y. S.; Henriksson, J.; Iliaš, M.; Jacob, Ch. R.; Knecht, S.; Komorovský, S.; Kullie, O.; Larsen, C. V.; Nataraj, H. S.; Norman, P.; Olejniczak, G.; Olsen, J.; Park, Y. C.; Pedersen, J. K.; Pernpointner, M.; Ruud, K.; Sałek, P.; Schimmelpfennig, B.; Sikkema, J.; Thorvaldsen, A. J.; Thyssen, J.; van Stralen, J.; Villaume, S.; Visser, O.; Winther, T.; Yamamoto S. *DIRAC13*, 2013, (see http://www.diracprogram.org).
(25) Dyall, K. G. *Theor. Chem. Acc.* **2007**, *117*, 483.
(26) Jensen, F. *J. Chem. Theory Comput.* **2008**, *4*, 719.
(27) Olejniczak, M.; Bast, R.; Saue, T.; Pecul, M. *J. Chem. Phys.* **2012**, *136*, 014108.
(28) te Velde, G.; Bickelhaupt, F. M.; van Gisbergen, S. J. A.; Fonseca Guerra, C.; Baerends, E. J.; Snijders, J. G.; Ziegler, T. *J. Comput. Chem.* **2001**, *22*, 931. Fonseca Guerra, C.; Snijders, J. G.; te Velde, G.; Baerends, E. J. *Theor. Chem. Acc.* **1998**, *99*, 391. ADF2014, SCM, Theoretical Chemistry, Vrije Universiteit: Amsterdam, The Netherlands; http://www.scm.com.
(29) Adamo, C.; Barone, V. *Chem. Phys. Lett.* **1997**, *274*, 242.
(30) van Lenthe, E.; Baerends, E. J. *J. Comput. Chem.* **2003**, *24*, 1142.
(31) Wolff, S. K.; Ziegler, T.; van Lenthe, T.; Baerends, E. J. *J. Chem. Phys.* **1999**, *110*, 7689.
(32) Reed, A. E.; Curtiss, L. A.; Weinhold, F. *Chem. Rev.* **1988**, *88*, 899−926.
(33) Glendening, E. D.; Badenhoop, J. K.; Reed, A. E.; Carpenter, J. E.; Bohmann, J. A.; Morales, C. M.; Landis, C. R.; Weinhold, F. Theoretical Chemistry Institute, University of Wisconsin: Madison, WI, 2013; http://nbo6.chem.wisc.edu/.
(34) (a) Bohmann, J. A.; Weinhold, F.; Farrar, T. C. *J. Chem. Phys.* **1997**, *107*, 1173−1184. (b) Autschbach, J.; Zheng, T. *Magn. Reson. Chem.* **2008**, *46*, S45. (c) Autschbach, J. *J. Chem. Phys.* **2008**, *128*, 164112. (d) Aquino, F.; Pritchard, B.; Autschbach, J. *J. Chem. Theory Comput.* **2012**, *8*, 598.
(35) (a) Zurek, E.; Pickard, C. K.; Autschbach, J. *J. Phys. Chem. C* **2008**, *112*, 11744. (b) Autschbach, J.; Zheng, S.; Schurko, R. W. *Concepts Magn. Reson., Part A* **2010**, *361*, 84.
(36) For reviews see for instance: (a) Brookhart, M.; Green, M. L. H. *J. Organomet. Chem.* **1983**, *250*, 395. (b) Brookhart, M.; Green, M. L. H.; Wong, L.L. *Prog. Inorg. Chem.* **1988**, *36*, 1. (c) Clot, E.; Eisenstein, O. *Structure. Bonding, Computational Inorganic Chemistry*; Kaltsoyannis, N., McGrady, J. E., Eds.; Springer Verlag: Heidelberg, 2004; Vol. *113*, p 1.

DOI: 10.1021/jacs.5b12597
J. Am. Chem. Soc. 2016, 138, 2261−2272

(37) For all complexes the shielding σ_{11} and its contribution σ_{xx} are essentially equal, Figures S11 and S12.
(38) It should be noted that the contribution of the empty orbitals is not explicitly given but can easily be assigned from the rotating orbital model.
(39) In particular, the 5d shell is destabilized by relativistic effects; tests calculations for the W complex removing scalar and SO effects on the metal give results relatively close to the Mo case, see Table S14 in Supporting Information.

DOI: 10.1021/jacs.5b12597
J. Am. Chem. Soc. 2016, 138, 2261−2272